Journal of Fluorescence, Vol. 14, No. 6, November 2004 (©2004)

Optical Characterization of Eu^{3+} Ions in CdSe Nanocrystal Containing Silica Glass

Gijo Jose,[1] G. Jose,[2] V. Thomas,[1] C. Joseph,[1] M. A. Ittyachen,[3] and N. V. Unnikrishnan[1,4]

Received January 14, 2004; revised June 12, 2004; accepted June 15, 2004

Silica glass samples containing CdSe/Eu^{3+} ions were prepared by sol-gel route. Size distribution and optical band gap of the nanoparticles were calculated from absorption spectrum. It is observed that the presence of CdSe nanocrystallites enhances the fluorescence of europium in silica glass. The phonon sideband spectrum associated with the excitation transition $^7F_0-^5D_2$ is used to analyze the electron–phonon coupling and nonradiative deexcitiation of the rare earth ions in the glass host. The observed fluorescence enhancement is discussed on the basis of phonon assisted energy transfer from electron-hole recombination of the CdSe nanocrystallites to the rare earth ion and multiphonon relaxation.

KEY WORDS: Rare earth doped silica glasses; nanocrystals; semiconductors; sol-gel process.

INTRODUCTION

Semiconductor nanocrystallites find application as laser emitters, storage devices, fluorescence markers and being used for many possible optical as well as photonic applications [1,2]. In semiconductor nanocrystals, not only the electronic energy levels but also the lattice vibrational modes become discrete due to the three dimensional confinement. The most enhanced values of nonlinearity have been found for photon energies, with respect to bandgap energy E_g, or between $E_g/2$ and E_g for optical communications [3]. The band gap of semiconductor quantum dots is dependent not only on the type of semiconductor, but also on the particle size, which causes quantum confinement "blue shift." Lanthanide ions have the fairly unique property of sharp spectral lines (4f–4f) in the solid phase. The spectral intensities of the trivalent lanthanide ions can be fine tuned by an appropriate choice of the medium in which the ion is embedded [4]. Optical transitions of rare earth ions, which are confined within the 4f level structure, have got crucial applications in optoelectronic technology [5]. Electron–electron and spin–orbit interactions dominate the electronic structure of the rare earth ions. Eu^{3+} is an excellent indicator of the site symmetry and chemical bonding in glasses since Eu^{3+} ions incorporated in low-symmetry sites exhibit enhanced f–f transition probabilities [6]. Knowledge of the local structure of the rare earth in hosts is valuable in optical devices like upconversion laser and laser induced holographic gratings [7]. In order to design the glass material with high efficiency it is better to select a glass matrix in which the maximum phonon energy is small i.e. the non-radiative loss due to multiphonon relaxation is small [8,9]. Sol-gel method is useful in the preparation of nanocrystallites doped gel glasses with relatively high particle concentrations, small particle diameter and uniform size distribution [10]. The sol-gel process allows incorporation of semiconductor nanocrystals along with rare earth elements at low temperatures with predetermined concentration and size. Transparent media, especially sol-gel glasses with complex composition are of interest for understanding the electronic excitation and

[1] School of Pure & Applied Physics, Mahatma Gandhi University, Kottayam 686 560, India.
[2] Department of Physics, Indian Institute of Technology Guwahati, Guwahati 781039, India.
[3] Department of Instrumentation, Cochin University of Science & Technology, Cochin 22, India.
[4] To whom correspondence should be addressed. E-mail: spapf@sancharnet.in

1053-0509/04/1100-0733/0

relaxation phenomena with participation of two and more active centers. [11,12]. In a recent communication [13] we have reported the fluorescence enhancement of Eu^{3+} ions in the presence of CdSe nanocrystallites. Here we present the analysis of phonon sideband and fluorescence of Eu^{3+} ions in sol gel silica matrix to probe the local structural evolution and its dependence on observed spectral intensities.

EXPERIMENTAL DETAILS

Europium doped and CdSe/Eu^{3+}co-doped silica glasses were prepared by the sol-gel process with tetraethyl orthosilicate (TEOS), cadmium acetate, selenic acid and europium nitrate in the presence of water and ethanol. We introduced Eu^{3+} ions into precursor sols within the framework of the modified sol-gel technique based on the catalytic hydrolysis of silicon–organic compounds with subsequent polycondensation of R–Si–O fragments. CdSe nanocrystallites were prepared from cadmium acetate and selenic acid by their decomposition reaction and incorporated into the SiO_2-matrix through annealing. Measured volumes of 1 M HCl were added as a catalyst. The mixture (sol) is poured into polypropylene containers, which is sealed and kept to form stiff gel. Eu^{3+}(3 wt%) CdSe(7 wt%)[Sample A], Eu^{3+}(3 wt%) [Sample B] and CdSe(7 wt%) [Sample C] doped silica samples were prepared. Variation in the annealing conditions resulted in stabilization of final products and provided a high mechanical strength of materials. The absorption spectrum is recorded using a spectrophotometer (Shimadzu-UVPC 2401). The excitation and luminescence spectra were taken using a spectrofluorophotometer (Shimadzu-RFPC 5301) for samples heated to 500°C. All measurements were done at room temperature (∼300 K)

RESULTS AND DISCUSSION

The absorption spectra corresponding to the CdSe doped silica sol-gel glass is given in Fig. 1. The direct absorption bandgap of the CdSe nanoparticles can be determined by fitting the absorption data to the equation

$$\alpha h\nu = B\left(h\nu - E_{\mathrm{g}}\right)^{1/2} \tag{1}$$

(shown in the inset of Fig. 1) in which $h\nu$ is the photon energy, α is the absorption coefficient, E_g is the absorption bandgap and B is a constant relative to the material. The absorption coefficient can be obtained from the equation $\alpha = \frac{2.303A}{d}$ where A is the absorbance and d is the

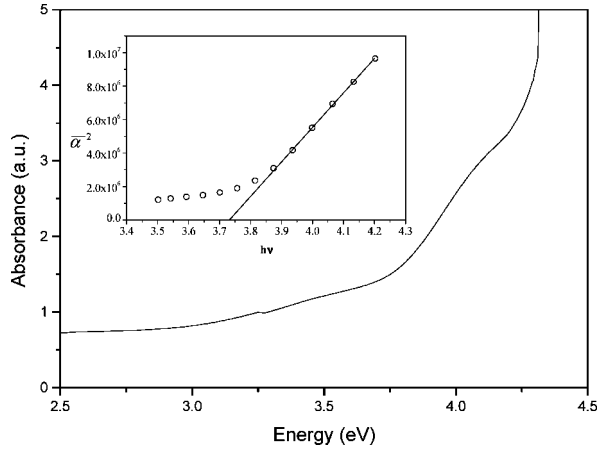

Fig. 1. Absorption spectrum of CdSe containing silica (Sample C). Inset show the $\bar{\alpha}^2$ vs. hν curve of (7 wt%) with x-axis in eV used to estimate bandgap CdSe nanocrystals.

thickness of the sample. It is well known that Rayleigh scattering from the nanoparticles can mask the features of the absorption spectrum to a certain extent. In order to account for the scattering phenomenon a correction factor given by [14]

$$\gamma = \frac{4}{9}V\left(\frac{\omega}{c}\right)^4 p\,(1-p)\,(\varepsilon_1 - \varepsilon_2)^2$$

has to be added to the observed absorption coefficient. In the above expression V is the volume of inhomogeneties responsible for scattering, p is the volume fraction of the inhomogeneties and ε_1 and ε_2 are the real parts of dielectric functions of the inhomogeneties and matrix respectively. The observed absorption coefficient then becomes the apparent absorption coefficient given by $\bar{\alpha} = \alpha + \gamma$. The plot of $\bar{\alpha}^2$ verses $h\nu$ [Fig. 1], gives the value of the bandgap as 3.73 eV. This is large compared to the bulk CdSe, a direct semiconductor, with bandgap energy of 1.7 eV [9,15]. Semiconductor nanocrystals are known to have an absorption edge, which is shifted with respect to the bulk material, toward shorter wavelengths [3]. The blueshift of the absorption edge can be explained by the effective mass approximation model, developed by Brus [16] and Kayanuma [17]. In the strong exciton confinement regime of nanoparticles (particle radius $< a_{\mathrm{b}}$*), the energy $E(R)$ for the lowest 1S excited state as a function of cluster radius (R) given by

$$E(R) = E_{\mathrm{g}} + \frac{\pi e a_{\mathrm{b}}^*}{8\varepsilon R^2} - \frac{1.786e^2}{4\pi\varepsilon R} + 2.48E_{\mathrm{R}} \tag{2}$$

where a_{b}*, Bohr radius of the exciton (for CdSe 5.6 nm), ε is the dielectric constant of the nanocrystallite (for CdSe, 8.98) and E_{R} is the bulk exciton Rydberg energy

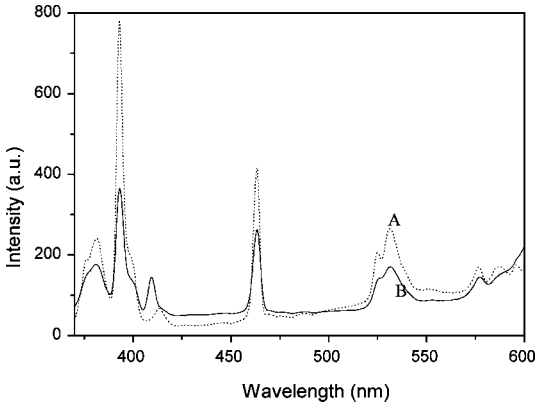

Fig. 2. Excitation spectra ($\lambda_{em} = 614$ nm) of samples A (dotted curve) and B (solid curve) heated to 500°C taken at room temperature.

(for CdSe 0.016 eV). The second term is the quantum confinement localization for the electrons and holes, which leads to the blueshift. The third term is the Coulomb term leading to red shift, while the fourth term gives the spatial correlation energy, which is small and of minor importance. From the blueshift results, we could estimate that the quantum confinement effect of our CdSe nanoparticles should be larger than the Coulomb effect. The band edge absorption in Fig. 1 is used to calculate the average size distribution of the CdSe nanoparticles in the silica matrix. The particle radius is found to be 1.487 nm from the absorption spectrum and using the Brus formula. For II–VI semiconductor nanoparticles the shoulder peak is associated with the size distribution properties of the nanoparticles. The less pronounced shoulder peak suggests a size distribution of more than 10% for our CdSe nanoparticles [18].

Figure 2 shows the excitation spectra taken with an emission wavelength of 614 nm for Eu doped and Eu/CdSe co-doped samples. The excitation spectrum is the true fingerprint of the characteristic absorption lines corresponding to $4f^n$–$4f^n$ transitions of europium ions, but not the semiconductor host lattice excitation band. The intense peak at 464 nm correspond to a rigid glassy network that is formed at comparatively low temperature in CdSe + Eu^{3+} doped gel glass as compared to the Eu^{3+} doped one. By heating the samples to 500°C the silica network strengthens and the coordination water molecules are substituted by SiO_4 tetrahedra. The broadening and splitting of spectral lines are also observed and are induced by the change in chemical environment of Eu^{3+} ions during heat treatment. Further, the ligand perturbation produces stark splitting of the ^7F_J levels [19].

Phonon sideband analysis is one of the most powerful tools to investigate the local vibrational environment around rare earth ions. For the Eu^{3+} ions, the multiphonon relaxation process is predominant between $^5D_{j(j=0-3)}$ levels and the radiative emission occurs from $^5D_0$ level. Therefore if the coordination ions are coupled with the Eu^{3+} ions, the phonon sideband can be observed on the high energy side of the $^7F_0$–^5D_j excitation [20,21]. The Eu^{3+} ion has a suitable transition $^5D_2 \rightarrow {}^7F_0$ to measure phonon sidebands because fluorescence excitation band of the pure electronic transition is observed as a single peak and the energy gap to the next higher level is quite large [22]. Figure 3a and b shows the phonon side band (PSB) spectrum, which is observed at the high energy side of the zero phonon line (ZPL, $^7F_0 \rightarrow {}^5D_2$) for Eu doped and Eu/CdSe co-doped samples respectively. The ratio of the intensity of the PSB and the intensity of ZPL gives the electron phonon coupling strength, "g"

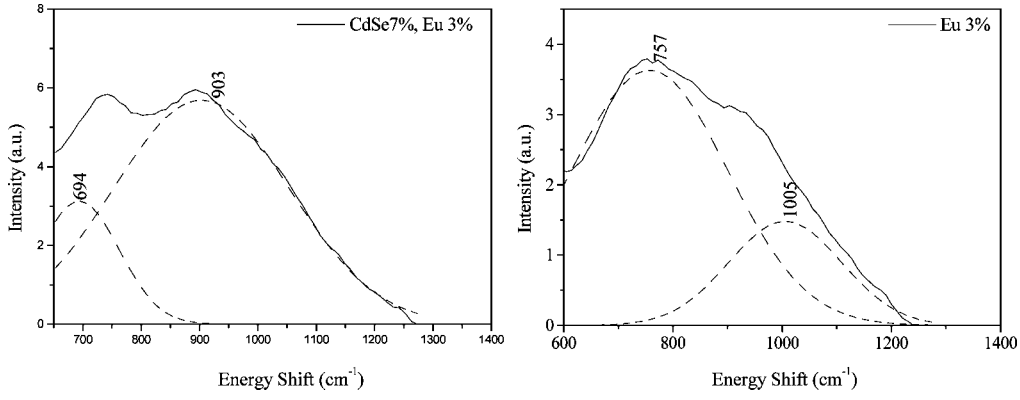

Fig. 3. Phonon sideband spectra of samples A (7% CdSe, 3% Eu) and B (0% CdSe, 3% Eu) heated to 500°C ($\lambda_{em} = 614$ nm) taken at room temperature. The dotted curves represent the deconvoluted spectra which is used to calculate the area under each peak.

[23–25]. It is found out for two peaks obtained by deconvoluting the broad PSB spectrum for the two samples as shown in the figures. The energy gap between the phonon sideband and the ZPL corresponds to phonon energy, $\hbar\omega$ in the neighborhood of Eu [26]. The energy gaps (ΔE) between the excited and ground state level for the excited energy levels $^5D_1$, $^5D_2$ and $^5D_3$ are approximated as 1750, 2500 and 2800 cm^{-1}, respectively [8]. The multiphonon relaxation rates are calculated using the values of g, $\hbar\omega$ and ΔE in the expression of Miyakawa and Dexter [27],

$$W_p(T) = W_o(0)\exp\left(-\Delta E\,\frac{\left[\ln\left\{\frac{p}{g(n+1)}\right\}-1\right]}{\hbar\omega}\right) \tag{3}$$

"p" the number of phonons consumed during multiphonon relaxation given by $p = \Delta E/\hbar\omega$. The $W_o(0)$ is the transition probability extrapolated to zero energy gap which is independent of the electronic nature of the rare earth ion [28] and "n" is the Planck's distribution function on the population of phonon as a function of temperature and phonon energy and is given by

$$n = \left(\exp\left(\frac{\hbar\omega}{kT}\right)-1\right) \tag{4}$$

The relevant data obtained for the Samples A and B, from the PSB analysis are collected in Table I. The efficiency of rare earth activated glasses is greatly dependent on the multiphonon relaxation rate of the excited rare earth ions. The multiphonon relaxation rate exponentially increases with increasing maximum phonon energy of the host matrix. The intra-configurational $4f^n$–$4f^n$ transitions are in the weak-coupling limit, and here the mediating phonon frequency does not differ greatly from the maximum phonon frequency. In Sample A the phonon sideband clearly shows two shoulders at around 903 and 694 cm^{-1}. In sample B the PSB shows two equally prominent peaks at ~1005 and ~757 cm^{-1} in the deconvoluted spectrum. The deconvolution procedure was adopted following the background correction of the recorded spectra (Fig. 3). These shoulders can be assigned based on the vibrational transitions given by the FTIR studies on gel derived silica glasses [29]. The peak around 1086 cm^{-1} corresponds to the Si—O—Si symmetric stretching in cyclic structures and it is found that in Sample B this is prominent. The peak at ~920 cm^{-1} is attributed to the non-bridging free broken Si—O bonds and by comparison with sample B we can see that it was generated in the host by the presence of CdSe. Vibrational energies of the SiO_4 unit in glasses range from 830–1060 cm^{-1} depending upon the number of non-bridging oxygens (NBO's) in the tetrahedron [23]. The CdSe acts as network modifiers at smaller concentrations, and this increases the NBO's and the band gets shifted to lower energies. The transition at ~757 cm^{-1} is prominent in sample B which represents the SiO_4 asymmetric stretching and Si—O—Si bending in SiO_2 mode vibrations. The extent to which a particular vibrational mode is coupled to an electronic transition is usually described by the electron–phonon coupling strength "g"[30]. The g value is higher in B for this phonon mode comparing the one at 962 cm^{-1} (see Table I). An increase in g with increase of CdSe is an indication of increasing covalency and/or a shortening of the Eu—O bond, and is observed as a shift of absorption band to smaller energies. In the case of sample A the multiphonon relaxation rate (for example from $^5D_1$) is an order of magnitude greater than that in sample B. The NBO's would probably increase the phonon density of the high frequency mode around rare earth ions. This suggests higher nonradiative decay to the emitting level $^5D_0$ from the higher energy levels of the excited europium ion and nonradiative phonon assisted energy transfer from the CdSe to Eu in Sample A. In the following discussion we are correlating this results to the observed increase in the fluorescence intensity of the Eu^{3+} in the presence of CdSe nanoparticles in the host.

Figure 4 presents the fluorescence spectra of the samples heated to 500°C recorded at room temperature with an excitation of 393 nm corresponding to the $^5L_6$ state of the Eu^{3+} ion. The main emission lines are due to the transitions from $^5D_0$ levels to the ^7F_j multiplets. No

Table I. Phonon Maxima ($\hbar\omega$), Electron Phonon Coupling Strength (g), Nonradiative Decay Rates for $^5D_1$, $^5D_2$, $^5D_3$ Ransitions of Eu^{3+} Ion in Sample A(CdSe 7%, Eu 3%) and Sample B(CdSe 0%, Eu 3%)

	$\hbar\omega$ (cm^{-1})		g								
Sample	Peak 1	Peak 2	Peak 1	Peak 2	Zero phonon line (cm^{-1})	$W_p(T)/W_o(0)$ from $^5D_1 \times (10^{-6})$		$W_p(T)/W_o(0)$ from $^5D_2 \times (10^{-6})$		$W_p(T)/W_o(0)$ from $^5D_3 \times (10^{-6})$	
A	694	903	0.00799	0.01456	21580	0.3556	74.805	0.2167	0.4122	0.000006088	0.02883
B	757	1005	0.01713	.006984	21580	7.026	53.77	1.673	0.2894	0.001951	0.04752

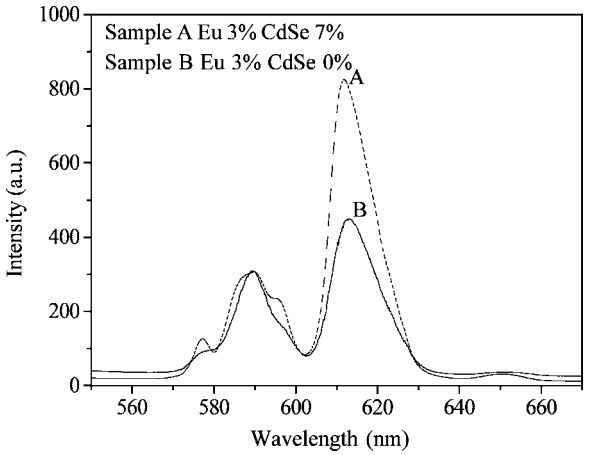

Fig. 4. Emission spectra of samples A (dotted curve) and B (solid curve) heated to 500°C ($\lambda_{ex} = 393$ nm) taken at room temperature.

emission was observed under this excitation for samples C. A considerable enhancement in the emission intensity of the $^5D_0 \rightarrow {}^7F_2$ transition is observed for CdSe+Eu^{3+}silica glass. The fluorescence intensity ratio of $^5D_0 \rightarrow {}^7F_2$ to $^5D_0 \rightarrow {}^7F_1$ transition indicates the degree of asymmetry in the vicinity of Eu^{3+} ions and Eu—O covalency which could be measured using the asymmetry ratio given as

$$\mathrm{AS} = \frac{\int I_{0\rightarrow 2} d\gamma}{\int I_{0\rightarrow 1} d\gamma} \tag{5}$$

where $I_{0\rightarrow j}$ denotes the intensity of $^5D_0 \rightarrow {}^7F_j$ transition. This ratio is influenced by the site symmetry, electronegativity and covalency of the ligand atoms. Larger the inequality of the emission intensities of the Eu^{3+} larger is the asymmetry and covalency effects. The J splitting becomes more apparent as the Eu^{3+} environment becomes more asymmetric. The asymmetry ratio (Table II) clearly indicates that the presence of nanocrystallites increases the covalency and the polarization in the local vicinities of the Eu^{3+}cations. A larger ratio corresponds to a more distorted or asymmetric local cation environment. This difference can be attributed to the change in chemical environment

Table II. Red to Orange Ratio (R/O) and Energy and FWHM for $^5D_0 \rightarrow {}^7F_0$ Transition of Eu^{3+} Ion in Sample A(CdSe 7%, Eu 3%) and Sample B(CdSe 0%, Eu 3%)

		$^5D_0 \rightarrow {}^7F_0$ emission	
Sample	Asymmetry ratio R/O	Energy (cm^{-1})	$\Delta\nu_{IH}$ (cm^{-1})
A	2.69	17337	338
B	1.45	17316	272

of Eu^{3+} in different media [20]. An increase of covalent bonding is responsible for a larger transition probability of the $^5D_0 \rightarrow {}^7F_2$ hypersensitive transition. The presence of CdSe in the nearest neighbor coordination of the Eu^{3+} changes the geometrical atomic arrangement as well as the bond strength. The incorporation of CdSe to the first coordination shell of Eu^{3+} would be responsible for a relative softening of the crystal field strength and in turn contributing to the distortion of the anion symmetry around the rare earth. This increase in covalency in the host lattice can be considered as an increase in the spatial extension of the electron wave functions of the rare earth ions and the ligands. The larger spatial extension of the 4f orbitals and the ligands enhances the electron phonon coupling strength. For stronger electron phonon coupling, faster multiphonon relaxation is expected [31]. This result supplements the observed electron–phonon coupling strength in Sample A corresponding to the phonon of frequency 912cm^{-1} and associated higher multiphonon relaxation rates (Table I).

The $^5D_0 \rightarrow {}^7F_0$ transition is nondegenerate and not subject to crystal field splitting changes in the vicinity of the Eu^{3+} ion. The position and line width of this 0–0 transition is a direct measure of the local bonding environment and the coordination of the Eu^{3+} ion [6]. The peak position of the $^5D_0 \rightarrow {}^7F_0$ transition is related to the nephelauxetic effect, which shifts the center of gravity of the J states. The shift to higher energy in the band maximum indicates that the chemical bond between Eu and ligands as strongly covalent for sample A compared to Sample B. Factors like local crystal fields, electron–phonon coupling and ion–ion interaction contribute to this broadening. Moreover the energy gap between $^5D_0$ state and the next lower $^7F_6$ state is about ten times the highest involved phonon energy. Therefore the probability of non-radiative deexcitation of the $^5D_0$ state by multiphonon process is very small [32]. Hence the improved efficient luminescence obtained in Eu/CdSe codoped silica glass can be attributed to the following interrelated properties. The reduction of concentration quenching (i.e. more dispersion of Eu ions in a medium with more NBOs as predicted by PSB analysis) for Eu:CdSe codoped silica glass compared to Eu doped sample. The nonradiative recombination of electron-hole pairs of the CdSe nanoparticles and phonon assisted transfer of energy to the emitting level of Eu as well as fast nonradiative decay from the higher energy levels of the Eu^{3+} ions will increase the population of the emitting levels and thereby enhancing the fluorescence from the rare earth ion. The photogenerated electron trapped in the CdSe strongly interacts with Eu^{3+} ion located close to the nanocrystallites in the SiO_2 matrix.

CONCLUSIONS

Nanometer sized CdSe crystallites along with Eu^{3+} ions were incorporated into silica matrix by sol-gel process. From the absorption spectra the average size of the CdSe nanocrystallites has been estimated to be between 4 and 7 nm. The values of the important parameters viz, phonon energy, multiphonon relaxation rate and electron phonon coupling strength were estimated from the PSB spectra for all the Eu doped samples. The analysis clearly predicts fluorescence enhancement in the CdSe/Eu codoped glass matrix. This observed stronger fluorescence could be correlated to the high phonon energy, phonon assisted energy transfer from the electron-hole recombination of the CdSe nano crystallites to the rare earth ion, multiphonon relaxation and rare earth distribution in the matrix containing CdSe nanocrystallites.

REFERENCES

1. M. C. Klein (1990). *Phys. Rev. B* **42**, 1123.
2. M. Nogami, T. Nagakura, and T. Hayakawa (2000). *J. Lumin.* **86**, 117–123.
3. E. J. C. Dawny, M. A. Fardad, M. Green, and E. M. Yeatman (1997). *J. Mater. Res.* **12**, 3115–3126.
4. M Nogami (2001). *J. Lumin.* **92**, 329–336.
5. T. Hayakawa, S. Tamil Selven, and M. Nogami (1999). *J. Non Cryst. Solids* **259**, 16.
6. C. Brecher and L. Riseberg (1976). *Phys. Rev. B* **13**, 81.
7. D. Levy, R. Reisfeld, and D. Anvir (1984). *Chem. Phys. Lett.* **109**, 593–597.
8. S. Todoroki, K. Hirao, and N. Soga (1992). *J. Non-Cryst. Solids* **143**, 46–51.
9. E. Lifshitz, I. Dag, I. Litvin, G. Hodes, S. Gorer, R. Reisfeld, M. Zelner, and H. Minti (1998). *Chem. Phys. Lett.* **288**, 188–196.
10. M. Zelner, H. Minti, R. Reisfeld, H. Cohen, Y. Feldman, S. R. Cohena, and R. Tenne (2001). *J. Sol-Gel Sci. Technol* **20**, 153.
11. S. Gorer, G. Hodes, Y. Sorek, and R. Reisfeld (1997). *Mater. Lett.* **31**, 209.
12. S. Tamil Selvan, T. Hayakawa, and M. Nogami (1999). *J. Phys. Chem. B* **103**, 7064.
13. G. Jose, G. Jose, V. Thomas, C. Joseph, M. A. Ittyachen, and N. V. Unnikrishnan (2003). *Mater. Lett.* **57**, 1051–1055.
14. S. A. Filonovich, Y. P. Rakovich, M. L. Vasilevskiy, M. V. Artemyev, D. V. Talapin, A. L. Rogach, A. G. Rolo, and M. J. M. Gomes (2002). *Mon.hefte Chem. Chem. Mon.* **133**, 909–918.
15. A. R. Kortan, R. Hull, R. L. Opila, M. G. Bawendi, M. L. Steigerwald, P. J. Carroll, and L. E. Brus (1990). *J. Am. Chem. Soc.* **112**, 1327–1332.
16. L. E. Brus (1983). *J. Chem. Phys.* **79**, 5566.
17. Y. Kayanuma (1998). *Phys. Rev. B* **38**, 9797–9805.
18. W. Dong and C. Zhu (2003). *J. Phys. Chem. Solids* **64**, 265.
19. Q. Guodong, W. Minquan, W. Mang, F. Xianping, and H. Zhanglian (1997). *J. Lumin.* **75**, 63–69.
20. S. Todoroki, S. Tanabe, K. Hirao, and N. Soga (1991). *J. Non-Cryst. Solids* **136**, 213–218.
21. M. Nogami and S. Ito (2000). *Phys. Rev. B* **61**, 14295-14298.
22. G. Vijaya Prakash (2000). *Mater. Lett.* **46**, 15–20.
23. H. Kuroda, S. Sionoya, and T. Kushida (1972). *Jpn. J. Appl. Phys.* **33**, 125.
24. T. H. Izumitani and H. Kuroda (1982). *J. Non-Cryst. Solids* **52**, 303–313.
25. G. Vijaya Prakash and R. Jagannathan (1999). *Spectrochim. Acta Part A* **55**, 1799–1808.
26. S. Tanabe, S. Todoroki, K. Hirao, and N. Soga (1990). *J. Non-Cryst. Solids* **122**, 59–65.
27. T. Miyakawa and D. L. Dexter (1970). *Phys. Rev. B* **1**, 2961–2970.
28. A. Boujaj, A. Monteil, C. Bovier, J. Serughetti, and M. Ferrari (1994). *J. Sol-Gel Sci. Technol* **2,** 771–774.
29. F. Rubio, J. Rubio, and J. L. Oteo (1998). *Spectrosc. Lett.* **31**, 199–219.
30. M. Wachtler, A. Speghini, S. Pigorini, R. Rolli, and M. Bettinelli (1997). *J. Non-Cryst. Solids* **217**, 111–114.
31. A. Meijerink, G. Blasse, J. Sytsma, and A. Ellens (1996). *Acta Phys. Pol. A* **90**, 109.
32. S. Todoroki, K. Hirao, and N. Soga (1992). *J. Appl. Phys.* **72**(12), 5853–5860.